Theory

Basis

We utilise a complete basis of the form, $\mathcal{B} = \{|\phi_i\rangle\}_{i=1}^{N}$, where the basis functions are represented in coordinate-space in the form

$$\phi_i(r, \Omega) = \frac{1}{r}\varphi_{k_i,\ell_i}(r)Y_{\ell_i}^{m_i}(\Omega) \quad \text{for} \quad i = 1, \ldots, N \tag{1}$$

where the radial functions, $\mathcal{R} = \{|\varphi_{k_i,\ell_i}\rangle\}_{i=1}^{N}$ form a complete basis for the radial function space, in the limit as $N \to \infty$. We utilise a Laguerre basis for the set of radial functions which, for $k = 1, 2, \ldots$ and where $\ell \in \{0, 1, \ldots\}$, are of the following form in coordinate-space

$$\varphi_{k,\ell}(r) = N_{k,\ell}(2\alpha_\ell r)^{\ell+1}\exp(-\alpha_\ell r)L_{k-1}^{2\ell+1}(2\alpha_\ell r) \tag{2}$$

where $\alpha_\ell \in (0, \infty)$ are arbitrarily chosen constants, where $N_{k,\ell}$ are the normalisation constants, given by

$$N_{k,\ell} = \sqrt{\frac{\alpha_\ell(k-1)!}{(k+\ell)(k+2\ell)!}} \tag{3}$$

and where $L_{k-1}^{2\ell+1}$ are the generalised Laguerre polynomials.

Overlap Matrix Elements

The overlap matrix elements, $B_{i,j}$, are of the form

$$B_{i,j} = \langle\phi_i|\phi_j\rangle = \langle\tfrac{1}{r}\varphi_{k_i,\ell_i}|\tfrac{1}{r}\varphi_{k_j,\ell_j}\rangle\,\langle Y_{l_i}^{m_i}|Y_{l_j}^{m_j}\rangle = \langle\tfrac{1}{r}\varphi_{k_i,\ell_i}|\tfrac{1}{r}\varphi_{k_j,\ell_j}\rangle\,\delta_{l_i,l_j}\delta_{m_i,m_j} \tag{4}$$

where

$$\langle\tfrac{1}{r}\varphi_{k_i,\ell}|\tfrac{1}{r}\varphi_{k_j,\ell}\rangle = \begin{cases} 1, & \text{if} \quad k_i = k_j \\ -\tfrac{1}{2}\sqrt{1 - \dfrac{\ell(\ell+1)}{(k_i+\ell)(k_i+\ell+1)}}, & \text{if} \quad k_j = k_i + 1 \\ \langle\tfrac{1}{r}\varphi_{k_j,\ell}|\tfrac{1}{r}\varphi_{k_i,\ell}\rangle, & \text{if} \quad k_i = k_j + 1 \\ 0, & \text{otherwise} \end{cases} \tag{5}$$

Kinetic Matrix Elements

The kinetic matrix elements, $K_{i,j}$, are of the form

$$K_{i,j} = \langle\phi_i|\hat{K}|\phi_j\rangle = \alpha^2(\delta_{k_i,k_j} - \tfrac{1}{2}\langle\tfrac{1}{r}\varphi_{k_i,\ell_i}|\tfrac{1}{r}\varphi_{k_j,\ell_j}\rangle)\delta_{l_i,l_j}\delta_{m_i,m_j}. \tag{6}$$

Spherically-Symmetric Potential Matrix Elements

For a spherically symmetric potential, $V(r, \Omega) = V(r)$, the potential matrix elements can be calculated numerically to be of the form

$$V_{i,j} = \langle\phi_i|\hat{V}|\phi_j\rangle = \langle\tfrac{1}{r}\varphi_{k_i,\ell_i}|\hat{V}|\tfrac{1}{r}\varphi_{k_j,\ell_j}\rangle\,\delta_{l_i,l_j}\delta_{m_i,m_j} \tag{7}$$

where

$$\langle\tfrac{1}{r}\varphi_{k_i,\ell_i}|\hat{V}|\tfrac{1}{r}\varphi_{k_j,\ell_j}\rangle = \int_0^\infty \mathrm{d}r\,\varphi_{k_i,\ell_i}(r)V(r)\varphi_{k_j,\ell_j}(r). \tag{8}$$

1 H_2^+ Potential-Energy Curves

Details of Relevant Theory and Code

Axially-Symmetric Potential

The axially-symmetric potential of the H_2^+ molecule, with two nuclei at $\mathbf{R} = (0, 0, \pm\frac{R}{2})$, can be written in the form

$$V(r, \Omega) = -\left(\frac{1}{\|\mathbf{r} + \mathbf{R}\|} + \frac{1}{\|\mathbf{r} - \mathbf{R}\|} \right) \tag{9}$$

which can be written alternatively, using the multipole expansion, in the form

$$V(r, \Omega) = -2 \sum_{\lambda \in E} \sqrt{\frac{4\pi}{2\lambda + 1}} \frac{r_<^\lambda}{r_>^{\lambda+1}} Y_\lambda^0(\Omega) \tag{10}$$

where $r_< = \min(r, \frac{R}{2})$, $r_> = \max(r, \frac{R}{2})$, and where $E = \{0, 2, 4, \ldots\}$ is the set of even integers. Note that in computational implementations, we truncate this sum at some term, $\lambda_{\max}$. Whence, it follows that the matrix elements for this potential can be calculated numerically to be of the form

$$V_{i,j} = \langle \phi_i | \hat{V} | \phi_j \rangle = -2 \sum_{\lambda \in E}^{\lambda_{\max}} \left(\int_0^\infty dr\, \varphi_{k_i, \ell_i}(r) \frac{r_<^\lambda}{r_>^{\lambda+1}} \varphi_{k_j, \ell_j}(r) \right) \left(\sqrt{\frac{4\pi}{2\lambda + 1}} \langle Y_{\ell_i}^{m_i} | Y_\lambda^0(\Omega) | Y_{\ell_j}^{m_j} \rangle \right) \tag{11}$$

$$\times\, \delta_{\pi_i, \pi_j} \delta_{m_i, m_j}$$

where $\pi_i = (-1)^{\ell_i}$ is the parity quantum number.

Basis Symmetry

Due to the axial symmetry of the H_2^+ potential, and thus the Hamiltonian for the electron in this molecule, we may choose a symmetrised basis $\mathcal{B}^{(m,\pi)}$ with specified azimuthal angular momentum, m, and parity, π. Furthermore, due to the computational constraints, we restrict our basis to having $\{N_\ell\}_{\ell=0}^{\ell_{\max}}$ radial functions per ℓ, with exponential falloffs $\{\alpha_\ell\}_{\ell=0}^{\ell_{\max}}$. For simplicity, we select $N_\ell = N_0$, and $\alpha_\ell = \alpha_0$, for each $\ell = 0, \ldots, \ell_{max}$.

Radial Grid

We utilise a radial grid of the form

$$\{r_i = d_r \cdot (i - 1)\}_{i=1}^{n_r} \tag{12}$$

with n_r is the smallest integer such that

$$d_r \cdot (n_r - 1) \geq r_{\max}. \tag{13}$$

Note that when we numerically evaluate matrix elements of potentials which are singular as $r \to 0$, we handle these integrals by searching for the first r_i for which $V_i = V(r_i)$ is non-singular and evaluating the integral from this point forwards.

2

Computational Parameters

Across all computations performed, we have utilised $\alpha = 1$, $\lambda_{\max} = 10$, $d_r = 0.1$ and $r_{\max} = 75$. Hence, to denote a selection of computational parameters, we shall use the notation

$$\mathcal{B}_{N_0, \ell_{\max}}^{(m, \pi)} \tag{14}$$

to indicate that the calculation has been performed with the Laguerre basis, with m, π symmetries, with N_0 radial functions per ℓ, and with $\ell = 0, \ldots, \ell_{\max}$.

Computational Procedure

The Hamiltonian for the H_2^+ molecule was diagonalised in the basis $\mathcal{B}_{N_0, \ell_{\max}}^{(m, \pi)}$, for $\pi \in \{-1, +1\}$, $m \in \{0\}$, $N_0 \in \{2^0, \ldots, 2^5\}$, and $\ell_{\max} \in \{0, \ldots, 6\}$, across a range of axial-distance values $R \in \{0.5, 1.0, \ldots, 10.0\}$.

1.1   Comparison with Accurate Potential-Energy Curve for $1s\sigma_g$.

The convergence of the H_2^+ potential-energy curve (PEC), for the $1s\sigma_g$ state, is shown for increasing $\ell_{\max}$ in Figure 1, and for increasing N_0 in Figure 2. It can be seen by comparing the two figures that increasing N_0 past a certain point does little to improve the accuracy of the PEC ($N_0 = 2^4$ and $N_0 = 2^5$ yield essentially identical PECs), while on the other hand, increasing $\ell_{\max}$ continues to yield improved accuracy of the PEC (at least up to $\ell_{\max} = 6$).

H_2^+ PEC, for $\mathcal{B}_{32,\ell_{max}}^{(0,+)}$ with varying ℓ_{max}, compared with `PEC.1ssg`.
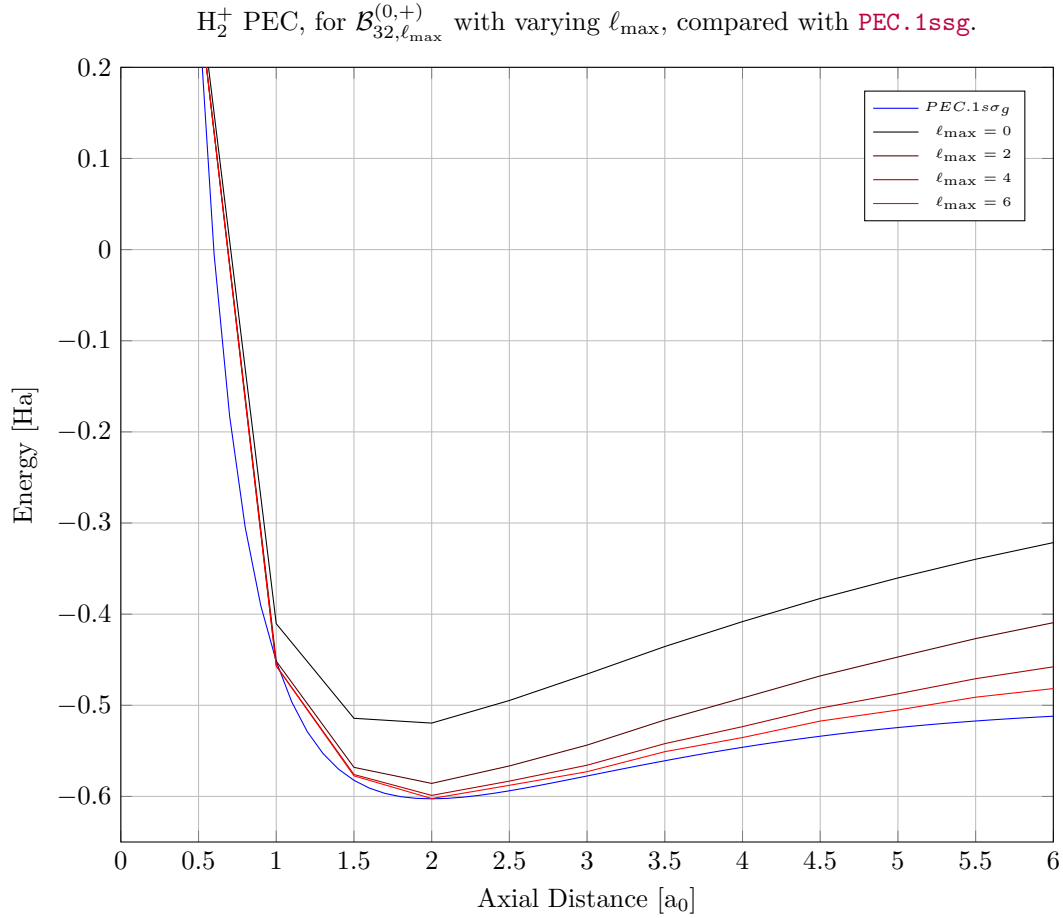

Figure 1: The potential energy curves, for $\ell_{max} = 0, 2, 4, 6$, obtained by diagonalising the H_2^+ Hamiltonian in the bases $\mathcal{B}_{32,\ell_{max}}^{(0,+)}$ (shown in black-to-red), are compared with the accuracte potential energy curve provided in `PEC.1ssg` (shown in blue). It can be seen that calculated PECs do converge to the accurate PEC, with a non-negligble increase in accuracy with increasing ℓ_{max}.
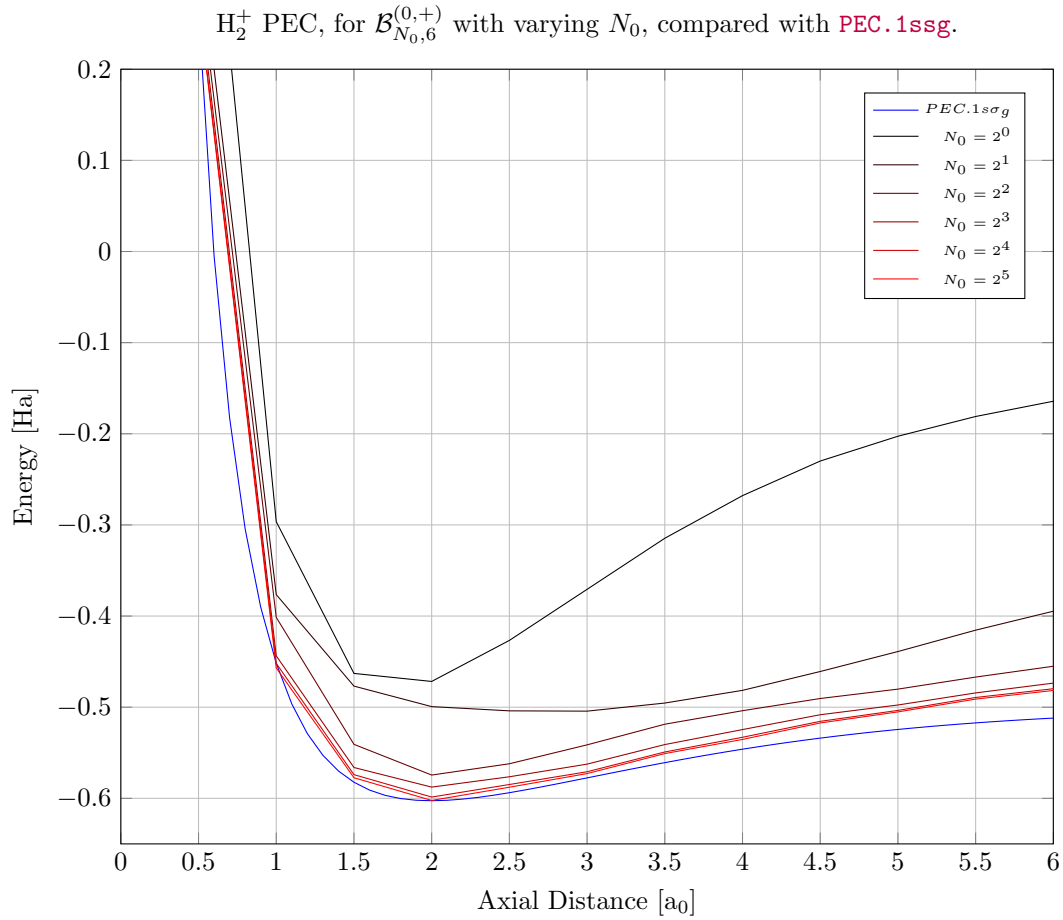
Figure 2: *The potential energy curves, for $N_0 = 2^0, \ldots, 2^5$, obtained by diagonalising the H_2^+ Hamiltonian in the bases $\mathcal{B}_{N_0,6}^{(0,+)}$ (shown in black-to-red), are compared with the accuracte potential energy curve provided in* PEC.1ssg *(shown in blue). It can be seen that calculated PECs do converge to the accurate PEC, however the computational cost increases dramatically for diminishing improvements in the accuracy of the PEC.*

1.2   Comparison with Accurate Potential-Energy Curve for $2p\sigma_u$.

The convergence of the H_2^+ potential-energy curve (PEC), for the $2p\sigma_u$ state, is shown for increasing ℓ_{max} in Figure 3, and for increasing N_0 in Figure 4. It can be seen by comparing the two figures that increasing N_0 past a certain point does little to improve the accuracy of the PEC ($N_0 = 2^4$ and $N_0 = 2^5$ yield essentially identical PECs), while on the other hand, increasing ℓ_{max} continues to yield improved accuracy of the PEC (at least up to $\ell_{max} = 5$).

H_2^+ PEC, for $\mathcal{B}_{32,\ell_{max}}^{(0,-)}$ with varying ℓ_{max}, compared with PEC.2psu.
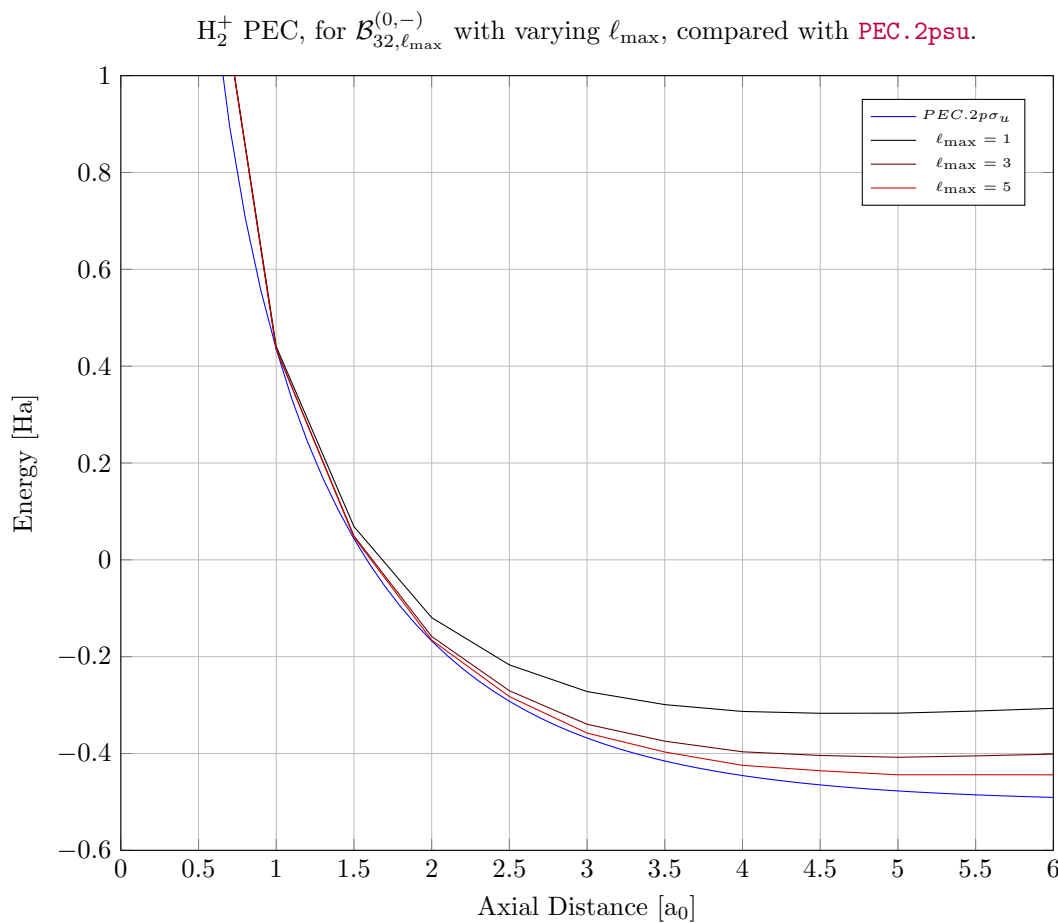

Figure 3: *The potential energy curves, for $\ell_{max} = 1, 3, 5$, obtained by diagonalising the H_2^+ Hamiltonian in the bases $\mathcal{B}_{32,\ell_{max}}^{(0,-)}$ (shown in black-to-red), are compared with the accuracte potential energy curve provided in* PEC.2psu *(shown in blue). It can be seen that calculated PECs do converge to the accurate PEC, with a non-negligble increase in accuracy with increasing ℓ_{max}.*

H_2^+ PEC, for $\mathcal{B}_{N_0,6}^{(0,-)}$ with varying N_0, compared with `PEC.2psu`.
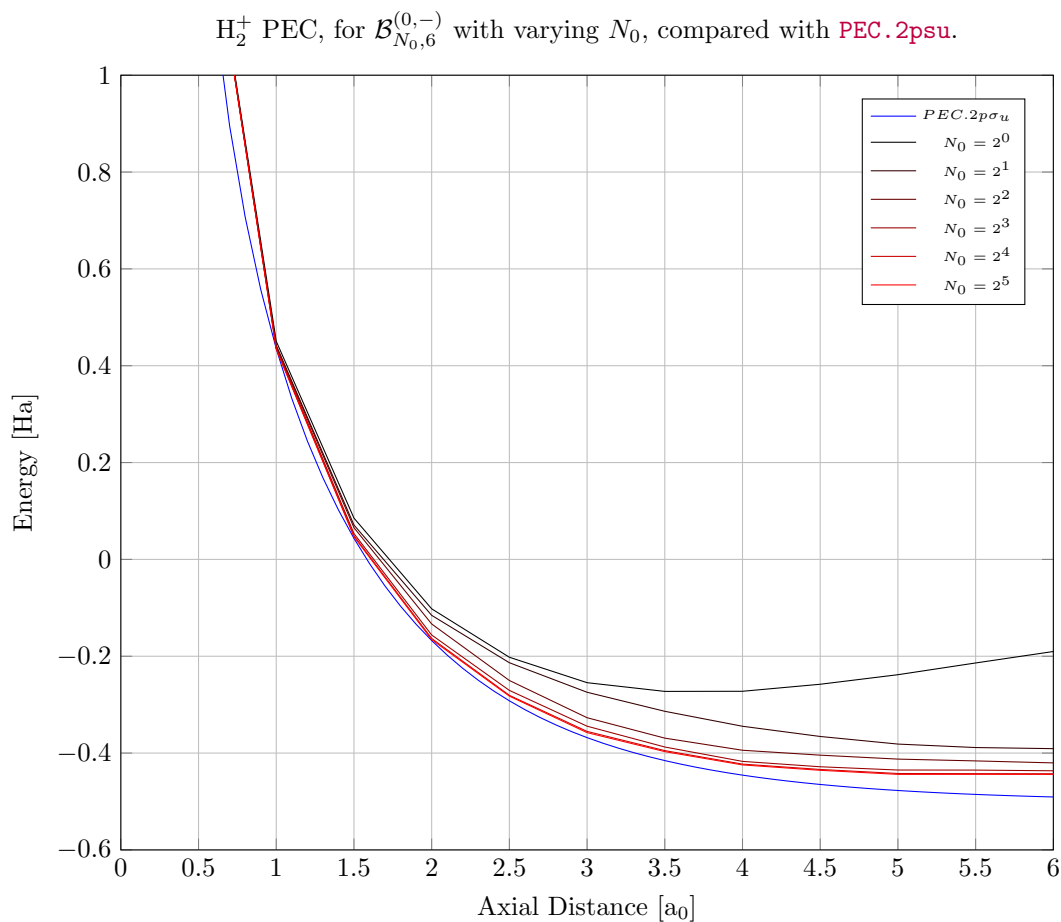

Figure 4: The potential energy curves, for $N_0 = 2^0, \ldots, 2^5$, obtained by diagonalising the H_2^+ Hamiltonian in the bases $\mathcal{B}_{N_0,6}^{(0,-)}$ (shown in black-to-red), are compared with the accuracte potential energy curve provided in PEC.2psu (shown in blue). It can be seen that calculated PECs do converge to the accurate PEC, however the computational cost increases dramatically for diminishing improvements in the accuracy of the PEC.

2 H_2^+ Vibrational Wave Functions

Details of Relevant Theory and Code

2.1 Vibrational Wave Functions for $1s\sigma_g$ PEC.

2.2 Lowest-Energy, $\nu = 0$, Vibrational Wave Functions for $1s\sigma_g$ PEC, for each Isotopologue of H_2^+.